Oxides of the 3*d* Transition Metals*

By F. J. MORIN

(Manuscript received April 16, 1958)

The magnetic, electrical and optical properties of the 3d metal oxides are examined for clues to the energy band structure. A tentative energy band scheme is proposed for the oxides of scandium, titanium and vanadium which suggests that the nonbonding 3d orbitals of neighboring cations overlap sufficiently to form a 3d conduction band. The 3d orbitals do not overlap in the oxides of the remaining 3d metals, with the consequence that the 3d electrons are in isolated energy states and electron transport occurs by electron exchange between cation neighbors and involves an activation energy. An energy level scheme for these latter oxides is calculated from simple electrostatics, and it is shown to agree with the observed electrical properties. Conduction in these oxides includes transport of high-mobility holes in the 2p band of the oxygen lattice and of low-mobility holes and electrons in the 3d levels of the cation lattice.

I. INTRODUCTION

The transition metals combine with other elements to form a host of compounds which are electronic conductors and which range in chemical bonding from ionic (oxides), through covalent (sulfides, arsenides) to metallic (carbides, nitrides). This range in valence character promises a great variety of energy band structures and transport processes and offers a rich field for theoretical and experimental investigation. No detailed determination of band structure or transport has been made for any of these compounds, and so they constitute an enormous gap in our knowledge of the solid state. Indeed, except for the 3*d* oxides, the semiconductor properties of transition metal compounds are largely unknown. In recent years the use of these oxides in electric[1] and magnetic[2] circuit elements and in heterogeneous catalysis,[3] as well as their importance in corrosion[4] have emphasized the necessity for a fundamental understanding of their properties. Now, from our point of view, the most fundamental aspect of a solid is its energy band structure. Therefore, it will

* This article is a chapter from *Semiconductors*, edited by N. B. Hannay, to be published by Reinhold Publishing Corp., New York, as part of the American Chemical Society Monograph Series.

be the concern of this paper to provide a tentative energy band scheme for the 3*d* oxides. The discussion will be restricted to the simple oxides and avoid the more complicated situations to be found in the oxide compounds, such as garnets, spinels and perovskites. Because of the scarcity of reliable experimental data on single-crystal material, the proposed scheme can only be regarded as tentative. At the same time, it provides a useful frame of reference for the planning and interpretation of future experiments.

We can begin by considering a relatively simple oxide, for example, zinc oxide, which is composed of ions having a closed-shell electronic configuration. The energy bands in zinc oxide arise, to a first approximation, from the filled 2*p* levels of the $O^{=}$ and the empty 4*s* levels of the Zn^{++} which are broadened when the ions are brought together to form the solid. The filled 2*p* band is separated from the empty 4*s* band by a forbidden energy region. Thus, zinc oxide is a semiconductor. In the same way, a 2*p* band and a 4*s* band are expected to arise in the 3*d* oxides. However, it is not easy to see what to expect from the partially filled 3*d* levels of the cations, and we must attempt to answer such questions as (i) whether the 3*d* wave functions overlap sufficiently to form a 3*d* band in any of the oxides or if they do not overlap, so that the 3*d* levels are localized energy levels, and (ii) the location in energy relative to the 3*d* levels (or band) of the 2*p* band of the anion lattice and the 4*s* band of the cation lattice.

To learn something about the properties of a 3*d* band it is instructive to consider the energy band situation in the 3*d* metals. Energy band calculations have been made for some of these metals, using the cellular and the tight binding methods.[5] Usually it is found that the 4*s* band is at least 10 ev wide and overlaps the 3*d* band, which in nickel, for example, is about 2.8 ev wide. On the other hand, the 3*d* band can hold ten electrons per atom, while the 4*s* band can hold only two electrons. This difference in numbers accentuates the difference in bandwidth: per electron, the 3*d* band in Ni is only $\frac{1}{15}$ as wide as the 4*s* band. The narrowness of the band means a high effective mass and low mobility for charge carriers in the band. In the metals, the electric current is carried largely by electrons in the 4*s* band, but these have their mobility decreased by transitions to the 3*d* band. In the 3*d* oxides, the increased internuclear distance can be expected to reduce the 3*d* bandwidth still further, because the overlap of the 3*d* wave functions will be greatly reduced. This will result in a further increase in effective mass and lowering of mobility. Later in this paper it is shown that the 4*s* band probably does not overlap

the 3*d* band in most of the oxides, so that electronic conduction can be entirely within the 3*d* band and thus involve carriers of very high effective mass and very low mobility. On the other hand, transport in a 4*s* or 2*p* band, should it occur, will probably be evidenced by the relatively high mobility of low-mass carriers in a wide band. Results of soft X-ray emission indicate the 2*p* band in oxides to be 10 to 20 ev wide.[6]

When the 3*d* band becomes extremely narrow it is no longer meaningful to assign a width to the band, and the 3*d* charge carriers can be considered to occupy energy levels localized on the cations. It was first pointed out by de Boer and Verwey[7] and by Mott[8] that this situation must exist in many oxides such as Cr_2O_3, Mn_2O_3, Fe_2O_3, CoO, NiO and CuO which are insulators when pure and stoichiometric and have room-temperature resistivities exceeding 10^{10} ohm-cm. In order that conduction in the 3*d* levels can occur there must be present, in pure NiO for example, some Ni^{+++} and Ni^{+} ions (electron hole pair) which can move about by exchanging electrons with the normal Ni^{++} of the lattice. These excited states, however, can only exist at high temperatures. Nickel oxide can be made conducting at room temperature by introducing Ni^{+++} ions into the lattice, either by a departure from stoichiometry (vacant Ni^{++} sites) or by the substitution of Li^{+} ions for Ni^{++} ions. Wandering of the Ni^{+++} about the Ni^{++} lattice by electron exchange is possible even though the cation separation of 3Å is twice the cation diameter. Transport of this type is expected to involve an activation energy associated with self-trapping of the charge carriers. Mobility will be extremely low and increase exponentially with temperature. Such behavior is distinctly different from transport in a band where mobility decreases with increasing temperature because of lattice scattering. Semiconductors in which transport is by electron transfer do not show many of the effects which have been used for study of the band structure and transport in semiconductors like silicon or germanium. For example, no Hall effect, photoconductivity or carrier injection is observable, so that transport measurements depend primarily upon Seebeck effect and electrical conductivity.

The oxides series to be considered in this paper is the following:

$$Sc_2O_3(d^0)\left|\begin{matrix}TiO(d^2)\\Ti_2O_3(d^1)\\TiO_2(d^0)\end{matrix}\right|V_2O_3(d^2)\left|Cr_2O_3(d^3)\right|Mn_2O_3(d^4)\left|\begin{matrix}FeO(d^6)\\Fe_2O_3(d^5)\end{matrix}\right|CoO(d^7)\left|NiO(d^8)\right|CuO(d^9)$$

The electronic configuration of the 3*d* shell is indicated. The 4*s* shell is assumed to be empty in all cases. The useful data concerning these oxides

are scant and most of them have been taken on ill-defined polycrystalline samples. However, from these data we shall try to derive a general energy band scheme for the 3*d* oxides. Particular attention will be paid to transport and optical absorption, because these properties give an indication of 3*d* bandwidth. Also, because the majority of the 3*d* oxides are antiferromagnets, any correlation between their magnetic and electric properties will be considered. In Section II a brief description of their magnetic properties is given. In Section III crystal field theory is discussed in a simple way and used to explain the available absorption spectra of the 3*d* oxides. In Section IV it is shown to be probable that a 3*d* band having appreciable width exists in the oxides of scandium, titanium and vanadium, whereas in the remaining oxides the 3*d* wave functions appear to be localized on the cations. In Section V the relative energies of the 4*s*, 3*d* and 2*p* levels are calculated. This energy level scheme is shown to fit fairly well the experimental results on NiO (Section VI) and Fe_2O_3 (Section VII). Finally, in Section VIII, a few speculations are made concerning transport in the localized 3*d* levels.

II. ANTIFERROMAGNETISM[9]

The transition metal oxides are antiferromagnetic, a state characterized by an ordered antiparallel arrangement of electron spins. Since the electronic structure of a solid underlies its magnetic as well as its semiconducting properties, it is not surprising that experiments on oxides have shown a connection between these two properties. Two ways of explaining magnetism have been used—the energy band approach for transition metals, and the ionic approach for transition metal oxides. In transition metals, the magnetic atoms lie close together and there is an interaction between the spin moments of neighbors. This *exchange interaction* depends upon the overlap of atomic orbitals. For atoms having a partially filled 3*d* shell the interaction may be either negative (antiparallel spins) or positive (parallel spins), depending upon interatomic distance, and changing from negative to positive with increasing distance. It is possible to divide an antiferromagnetic metal crystal into two magnetic sublattices, with each atom having nearest neighbors of opposite spins. The situation is different in transition metal oxides. In these, the magnetic cations are separated by anions. An example of this is MnO, whose sodium chloride structure is shown in Fig. 1. It is impossible for atom A' to have a spin direction antiparallel to that of all of its nearest neighbors, since one half of these B', C' and D' neighbors must have parallel spins to give an equal number of up and down spins in the lattice. There is one spin ordering, however, in which A' is antiparallel

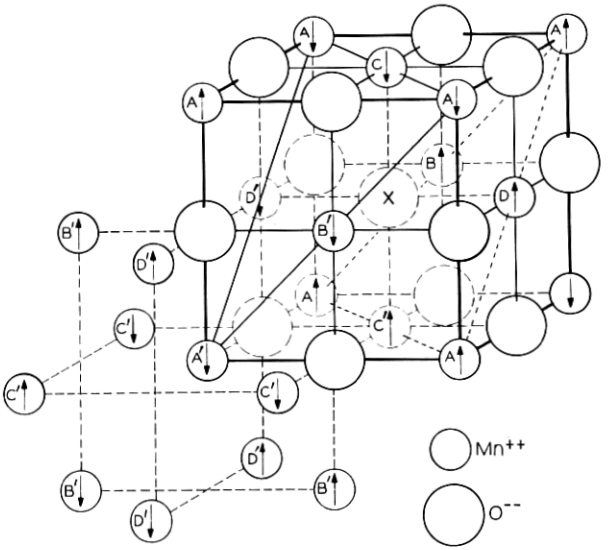

Fig. 1 — The sodium chloride structure and antiferromagnetic spin alignment in MnO. Spins in a (111) plane are parallel, with the (111) planes coupled antiparallel to each other. (After Gorter, Ref. 2.)

to all of its *next* nearest neighbors; this is shown in Fig. 1, and is the one actually found by neutron diffraction.

But now the antiparallel magnetic ions are separated by anions and the problem is to explain how exchange interaction can occur when electron orbits do not overlap. One way of approaching the problem was suggested by Slater.[5] Because of the exclusion principle, electrons of like spin will tend not to occupy the region between anion and cation. That is, electrons with + spin on a cation will repel electrons with + spin on the neighboring anion somewhat more than electrons with − spin. This repulsion will deform the outer electronic shell of the anion. In Fig. 1 it can be seen that anion X, for example, has three Mn^{++} neighbors (C', B, D) in a (111) plane (dotted diagonals) and having + spin. Anion electrons with + spin will tend to collect on the side of the anion opposite from this plane of cations. This tendency will be aided if the (111) plane (solid diagonals) of cations (C, D', B') on the opposite side of X have − spins, and it may be seen in Fig. 1 that this is the case. Thus, the antiferromagnetic alignment between spins in the (111) planes represents a lower energy state than does the ferromagnetic alignment. A different quantitative description of the coupling between electron spins of two cations separated by an anion has been given by

Anderson[10] and by Yamashita and Kondo.[11] It is called *superexchange*. Since the p orbitals of the anion are directed 180° apart, exchange is found to be strongest when cations are on opposite sides of the anion and weakest when they are at 90° from the anion.

At high temperature, thermal vibrations prevent the antiparallel ordering of spins, and the material is paramagnetic. The transition temperature separating the paramagnetic and antiferromagnetic states is called the Néel temperature, T_N. A plot of T_N as a function of the number of spins per cation is given in Fig. 2 for the oxides which are of interest in this chapter. The transition at T_N is characterized by the occurrence of maxima in specific heat, magnetic susceptibility and the expansion coefficient. Electron spin resonance disappears below T_N. The direction of spin alignment can be determined by neutron diffraction and magnetic susceptibility, using single crystals.

In the rhombohedral sesquioxides Ti_2O_3, V_2O_3, Cr_2O_3 and Fe_2O_3 the cations are in pairs of closely spaced parallel layers, each pair of layers separated from the next pair by a layer of oxygen ions. The spatial arrangement of the ions projected onto a plane is shown in Fig. 3. Cation layers are represented by solid horizontal lines and anion layers by dotted horizontal lines. The heavy lines show how four cations are coordinated with each anion. Each cation participates in 18 cation-

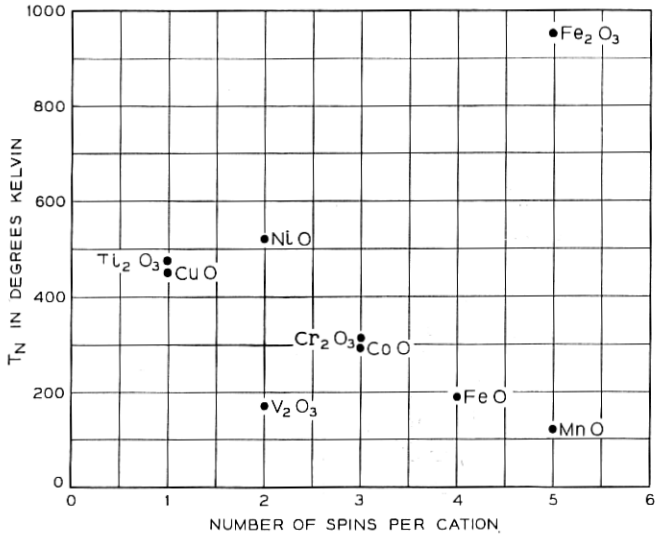

Fig. 2 — Plot of Néel temperature, T_N, against the number of spins per cation for some of the 3d oxides discussed in this paper.

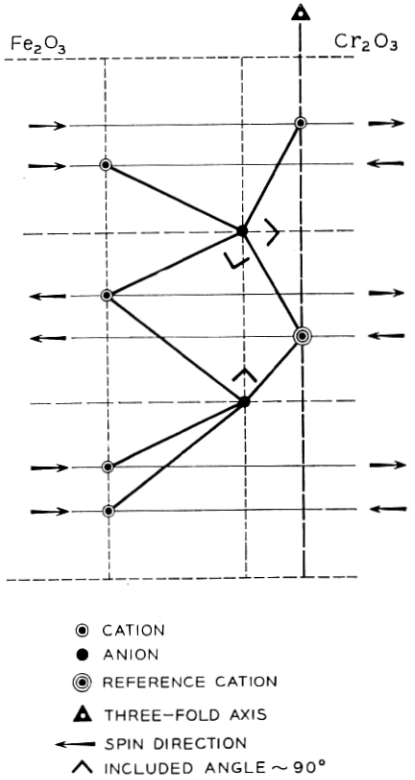

Fig. 3 — A projection onto a plane of the spatial arrangement of a group of ions in the rhombohedral sesquioxides. Cation layers are represented by solid lines and anion layers by dotted horizontal lines. The spin orientations of the cation layers are shown for Fe_2O_3 and Cr_2O_3. The cation-anion-cation paths of superexchange are indicated by the heavy lines which do not include a 90° angle. (After Gilleo, Ref. 35.)

anion-cation configurations, one-third of which are shown in Fig. 2. Because half of the configurations include an angle of about 90°, only nine configurations are important in exchange interactions. The spin alignment shown in Fig. 3 was found by neutron diffraction[12] and by magnetic susceptibility.[13] Spin alignment has not been determined in Ti_2O_3 and V_2O_3.

A second magnetic transformation is possible in the rhombohedral sesquioxides; that is, a change in the direction of spin alignment from perpendicular to the three-fold axis, as in Fig. 3, to parallel to this axis. According to neutron diffraction,[12] magnetic susceptibility[14] and spin

resonance,[15] this transformation occurs between $-30°C$ and $-15°C$ in Fe_2O_3.

Another interesting property of Fe_2O_3 is its weak ferromagnetism,[16] which persists up to T_N and has been explained on the basis of symmetry considerations.[17] The internal magnetic field due to the ferromagnetism produces an anomalous Hall effect,[18] which depends upon the magnetization of the material and disappears above T_N. This Hall effect probably can be understood on the basis of the theory[19] for a similar effect found in the transition metals. It cannot be used as a measure of carrier concentration in the usual way.

Exchange interaction, besides producing spin alignment, also tends to move the ions in such a way as to increase the exchange, and thus it causes lattice deformation. The net number of antiparallel neighbors increases with decreasing temperature because the opposing effect of thermal vibration decreases; correspondingly, lattice deformation increases with decreasing temperature. At temperatures below T_N, the exchange coupling between the (111) planes of spin cause rhombohedral distortion in MnO, FeO and NiO and tetragonal distortion in CoO.[20] Lattice distortion below T_N is also found in the rhombohedral sesquioxides. The exchange coupling between the cation layers contracts the lattice along the trigonal axis[21] but does not change the symmetry.

III. ATOMIC ORBITALS AND THE CRYSTAL FIELD[22]

If the $3d$ wave functions in an oxide do not overlap to form an energy band but remain concentrated near the cation, the cation, in effect, is isolated. It experiences, to a first approximation, only the electrostatic field due to the surrounding oxygens. Such a situation exists in the hydrated salts of the transition metals, for example the complex $Ni(H_2O)_6^{++}$, where the cation is surrounded octahedrally by six H_2O molecules with the oxygens (the negative end of the water dipole) nearest the cation. Similarly, in NiO, which is a face-centered cubic structure, the negative oxygens are also arranged in a regular octahedron about the Ni^{++}. In fact, the optical absorption spectrum for NiO is very similar to that for the hydrated salt. Therefore, these considerations suggest that the same theories might be applied to the $3d$ oxides as have been used in recent years to explain the optical properties of complex salts of $3d$ ions. Conversely, this implies that, if a given oxide spectrum can be understood in this way, the $3d$ wave functions in that oxide are concentrated near the cation and do not overlap to form a band. Accordingly, we will now see what available spectra indicate as to the possible existence of $3d$ bands.

Three theories have been used to account for the properties of the complexes:

1. molecular orbital,[23]
2. valence bond,[24]
3. crystal field.

The advantage of the crystal field theory is that it can give information in a simple way about the excited states of the cation. Thus, it furnishes an explanation of the absorption spectra and promises to give insight into the electric and magnetic properties of the oxides.

The crystal field theory assumes a purely ionic model and considers the effect of the octahedrally coordinated negative anions on the $3d$ electrons of the central cation. The geometry of the cation and its surroundings is shown in Fig. 4. Suppose, at first, that the central ion has a single $3d$ electron with the quantum numbers $l = 2$, $s = \frac{1}{2}$. There are five $(2l + 1)$ d orbits, all having the same energy in the isolated ion. The associated wave functions can be expressed as a function of radius, r, multiplied by functions with angular variation of the form xy/r^2, yz/r^2, zx/r^2, $(x^2 - y^2)/r^2$ and $(2z^2 - x^2 - y^2)/r^2$. These orbitals can be represented by the charge cloud distributions shown in Fig. 5. The xy, yz and zx orbitals are designated as $d\epsilon$ and the other orbitals as $d\gamma$. When negative anions are on the x, y, z axes, the negative charge clouds of the electrons in the $d\gamma$ orbitals, which are directed at the anions, are

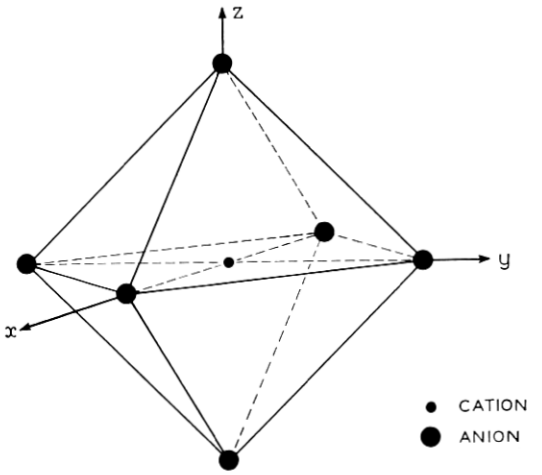

Fig. 4 — A regular octahedron of anions surrounding a central cation.

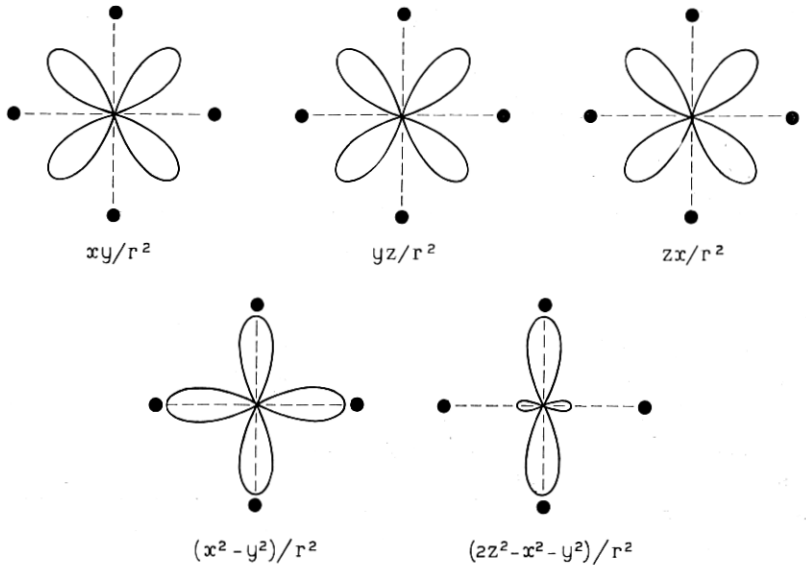

Fig. 5 — Angular distribution of the five 3*d* orbitals.

repulsed by the charge cloud of the anion. Thus, the $d\gamma$ orbitals have a higher electrostatic energy than the $d\epsilon$ orbitals, which are directed between the anions, and the ground state of the central ion is split as shown by the energy level diagram Fig. 6. This diagram is for an anion arrangement having cubic symmetry, which occurs in the rock salt oxides, and trigonal symmetry, which occurs in the rhombohedral sesquioxides. The trigonal case, since it involves a regular octahedron of anions, yields nearly the same excited states as does a cubic field, with an additional broadening of the absorption bands due to the small splitting of the $d\epsilon$ levels shown.

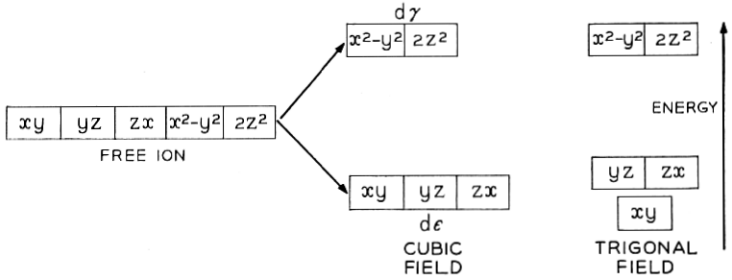

Fig. 6 — The ground state configuration of the five 3*d* orbitals: when in the free ion; in a crystal field of cubic symmetry (as in MnO, FeO, CoO and NiO); in a crystal field of trigonal symmetry (as in the rhombohedral sesquioxides).

An important rule concerning the splitting of these levels is that their centers of gravity in energy are not altered by the perturbation. That is,

$$3E_\epsilon + 2E_\gamma = 0. \tag{1}$$

Fixing the energy scale to be zero at the ground state of the free ion and defining 10 Dq as the energy difference between the two levels which a single 3d electron can occupy when subjected to a cubic field gives, from (1)

$$E_\epsilon = -4Dq, \tag{2}$$

$$E_\gamma = +6Dq. \tag{3}$$

The relative positions of the excited states above the ground state, as determined for ions with electron configurations d^1 to d^9 subjected to a cubic field, are shown in Fig. 7. To the left in each diagram are shown the free ion ground states, labeled with their term symbols. In diagrams (c) and (d) are also shown the first free ion excited states having the same spin multiplicity as the ground states, and in (b) two excited levels for the free ion are depicted. To the right in each diagram are shown the ground state and excited states for the ions in the solid, as produced by a cubic crystal field of strength Dq. Configuration d^5, shown in (b), is plotted in a different way (after Orgel[25]) from the other configurations, because its excited states but not the ground state are split. In these diagrams, the first excited state of the ion corresponds to the excitation of an electron from the $d\epsilon$ to the $d\gamma$ levels. For example, in NiO, configuration d^8, the first excited state of the nickel ion is due to the electronic transition represented by the change in configuration $d^6\epsilon\, d^2\gamma \rightarrow d^5\epsilon\, d^3\gamma$, which leaves a hole in the normally filled $d\epsilon$ levels. The energy of these two states can be calculated as follows. The ground state, $d^6\epsilon\, d^2\gamma$, is located at $(-4Dq \times 6 + 6Dq \times 2) = -12Dq$. The excited state, $d^5\epsilon\, d^3\gamma$, is located at $(-Dq \times 5 + 6Dq \times 3) = -2Dq$. These energy levels are shown in Fig. 7(d). These transitions became allowed as a result of lattice vibrations[26] and hemihedral distortion.[27]

The available absorption spectra for some of the oxides are shown in Fig. 8, together with the location of the absorption maxima of a hydrated salt of the cation in aqueous solution. The close correspondence between maxima found in hydrated complex and oxide for Fe^{+++} and Ni^{++} indicates that the cation is isolated in the oxide as it is in the hydrated salt, and suggests that the 3d wave functions do not overlap in the oxides of the metals iron and nickel. The spectra of Cr_2O_3, however, show a slight shift to frequencies lower than that of the hydrated

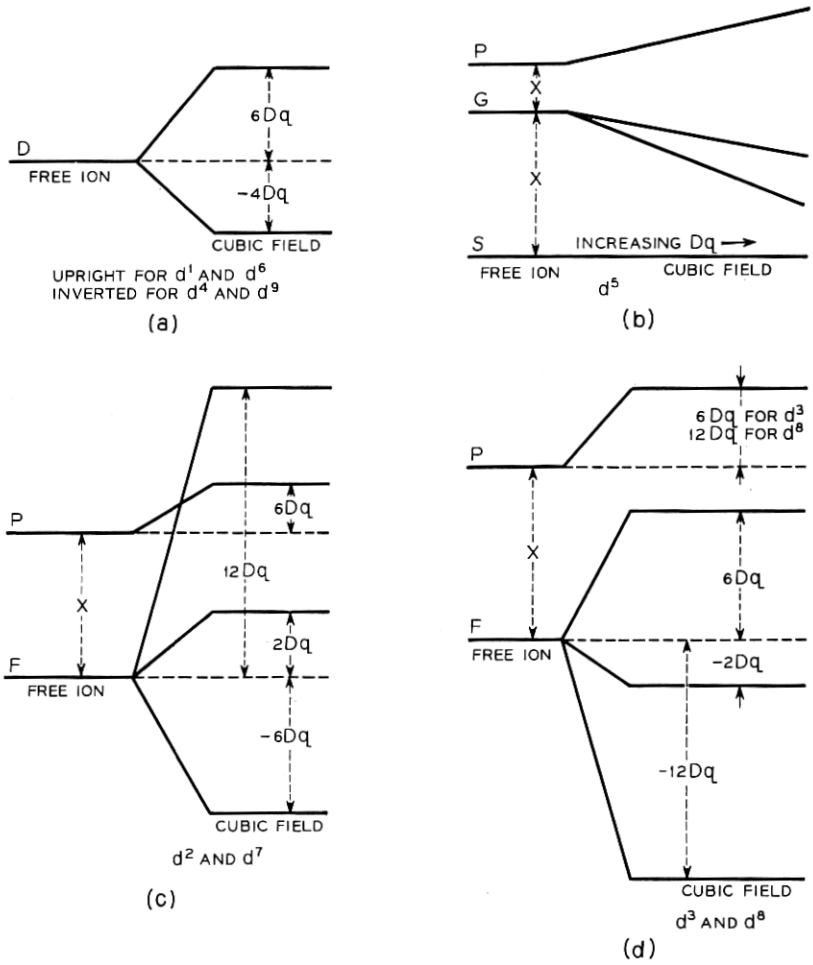

Fig. 7 — Positions of some excited states above the ground state for ions with electron configurations d^1 to d^9. In each diagram the free ion is to the left and labeled with appropriate term symbols, the ion in a cubic field is to the right.

salt, indicating a slight overlap of the 3*d* wave functions. This shift becomes very large in the spectra of Ti_2O_3, probably indicating that the cations in this oxide are not isolated as in their hydrated salts, and may be due to the overlap of 3*d* orbitals, with the formation of a 3*d* band.

From the spectra, the energy level diagrams of Fig. 7, and the values for the free ion excitation energies, X (from Ref. 28), the information given in Table I is obtained. The observed frequencies in the oxides,

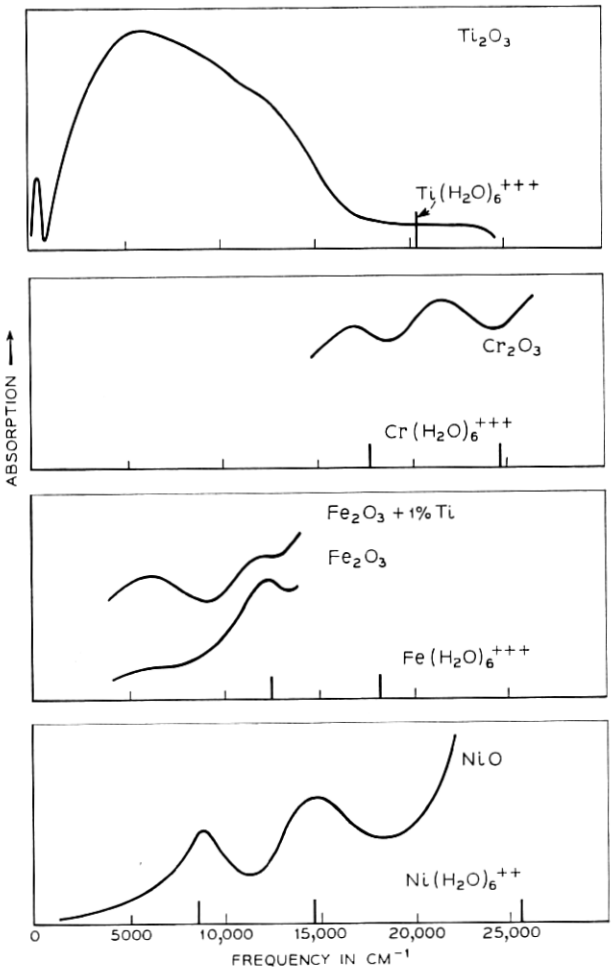

Fig. 8 — Absorption spectra for Ti_2O_3, Cr_2O_3, Fe_2O_3 and NiO compared to the location of absorption bands for hydrated salts of the corresponding cations. (Ti_2O_3 spectra after Pearson, Ref. 32; Cr_2O_3 spectra after D. S. McClure, unpublished; hydrated salt spectra after Holmes and McClure, Ref. 43.)

shown in Column 3, were used to calculate the values of Dq in Column 4. In turn, these were used to obtain the calculated frequencies in the final two columns.

Another bit of information can be obtained from the absorption spectrum of Fe_2O_3 containing titanium, Fig. 8, which shows an additional absorption band appearing at 6100 cm^{-1} when one per cent titanium is added substitutionally. Titanium is a donor in Fe_2O_3 and, in

TABLE I — SPECTRA OF OXIDES AND HYDRATED SALTS

Ion	Type of Comparison of Spectra	Frequencies			
		ν_1(cm^{-1})	Dq(cm^{-1})	ν_2(cm^{-1})	ν_3(cm^{-1})
Ti^{+++}	exp.	6000	—	—	—
	calc.	—	600	—	—
	aq.	20300	—	—	—
V^{+++}	aq.	17800	—	25700	—
Cr^{+++}	exp.	16800	—	21300	>27000
	calc.	—	1680	24000	30000
	aq.	17600	—	24700	—
Fe^{+++}	exp.	12200	—	>15500	—
	aq.	12600	—	18200	24500
Ni^{++}	exp.	8600	—	15400	>22000
	calc.	—	860	15500	26000
	aq.	8600	—	14700	25500

Comparison of spectra of oxides: exp. (measured); calc. (calculated from oxide data and diagrams Fig. 7); aq. (measured on hydrated salts). Data for the hydrated salts were taken from O. G. Holmes, and D. S. McClure.[43]
Note: 1 ev = 8100 cm^{-1}

this concentration, it is nearly all ionized to give Ti^{++++} and Fe^{++} ions. This absorption band, therefore, is probably due to the Fe^{++} ions, so that, from this information, Dq is 610 cm^{-1} for the Fe^{++} environment in Fe_2O_3. Now the value of Dq for Fe^{++} in $Fe(H_2O)_6^{++}$ is 1000 cm^{-1}, which can also be taken to be the value of Dq in FeO. The smaller value found for the Dq of Fe^{++} in Fe_2O_3 suggests that the anions surrounding the Fe^{++} ion are at a greater distance from the Fe^{++} ion in Fe_2O_3 than in FeO. This is just what one would expect to find if the conduction electron (Fe^{++}) in Fe_2O_3 polarized (repulsive polarization) the surrounding lattice.

IV. THE 3d BAND

The inner electronic configuration of the 3d metals is that of argon. As electrons are added to the argon core to build up the series, the nuclear charge is also increased. The electron cloud is thus subjected to an increasing nuclear charge but, on the other hand, the mutual repulsion of the electrons increases. The over-all decrease in ionic radius going from Ca^{++}(r = 0.99Å) to Zn^{++}(r = 0.83Å) indicates that nuclear attraction predominates over mutual repulsion, and the electron cloud becomes contracted. Therefore, if 3d wave functions overlap sufficiently to form a band in any 3d oxides, such band formation is to be expected at the beginning of the 3d series. Since, in fact, oxides such as Cr_2O_3, Fe_2O_3 and NiO normally are insulators, it is in the oxides of Sc, Ti and V that a 3d band might be expected. In the previous section it was sug-

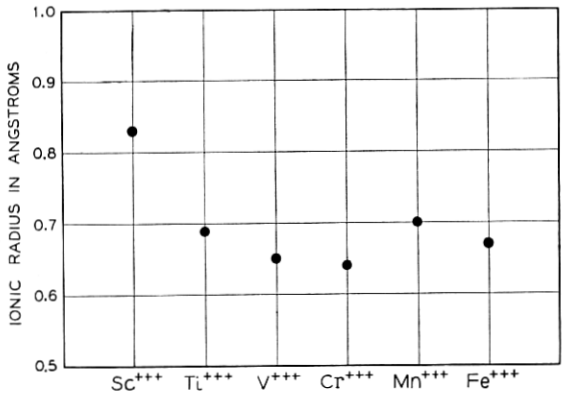

Fig. 9 — The rapid decrease in ionic radius with increasing atomic number for the first few members of the 3*d* series. This implies a contraction in the 3*d* wave functions and, therefore, a decrease in the amount by which they may overlap to form a 3*d* band. (Ionic radii from Goldschmidt, Ref. 44).

gested, on the basis of optical absorption, that there was evidence that such might be the case in Ti_2O_3. A comparison of the ionic radii of the trivalent cations plotted in Fig. 9 shows how rapidly the radius (and therefore the extent of the 3*d* wave functions) decreases with increasing atomic number in the first three members of the series. The abrupt increase in the radius of Mn^{+++} does not contradict this idea, since it is due to the addition of the first $d\gamma$ electron. This, since it interacts with the electron cloud of the anion, increases the effective radius of the cation.[29] Since no transport information exists for Sc_2O_3, the data for the oxides of Ti and V will be examined for evidence of a 3*d* band.

4.1 *TiO_2* (*Configuration* d^0)

In TiO_2, the electronic configuration of Ti^{++++} is $3d^0$, so that if a 3*d* band exists we expect it to be normally empty. We have, however, the possibilities of supplying electrons to the 3*d* band by excitation from imperfections or from the filled 2*p* band. Hall mobility of conduction electrons has been measured by Breckenridge and Hosler[30] in ceramic and single-crystal samples of TiO_2 (rutile). The electrons were thermally excited from lattice defects introduced by slight reduction of the samples. Room-temperature mobility ranged from 0.1 to 1.0 cm^2/volt-sec for all samples, the crystals tending to have the higher values. The mobility decreased in a normal way with increasing temperature. This mobility is 100 to 1000 times smaller than the electron mobility found in ZnO, and is precisely what is expected from transport in a 3*d* band.

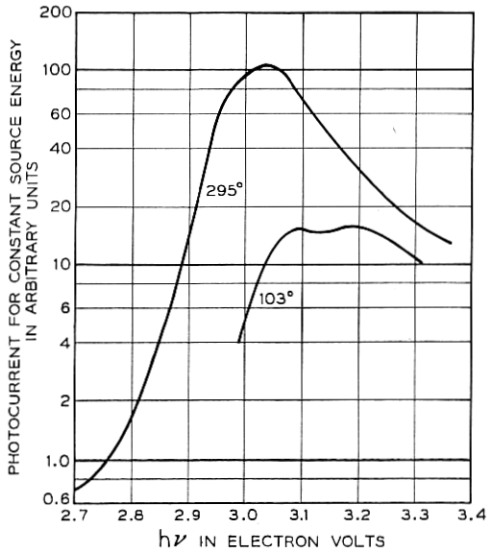

Fig. 10 — Photoconductivity in stoichiometric single crystal rutile. (After Cronemeyer, Ref. 31.)

Conductivity, photoconductivity and optical absorption have been measured by Cronemeyer[31] on pure stoichiometric single crystals of rutile. These data indicate an intrinsic forbidden energy gap of 3.05 ev. Above 1200°K, however, the conductivity temperature dependence suggests an increase in the energy gap to 3.67 ev. Presumably, the 3.05 ev represents an electronic transition from the filled $2p$ band of the oxygen lattice to the empty $3d$ band, which was indicated by Hall mobility to be the conduction band. The increase in the energy gap by as much as 0.6 ev at high temperature, suggests two possibilities: either the $4s$ band of Ti^{++++} is near the upper edge of the $3d$ band, and transitions to that band are also important, or the $3d$ band is split into two sub-bands. Discussion in Section V shows that the $4s$ band is probably too high in energy to play a role in conduction in the oxides. The second alternative —splitting of the $3d$ band into $d\epsilon$ and $d\gamma$ sub-bands—seems to be the most likely.

The photoconductivity data, Fig. 10, only extend to 3.4 ev, presumably not high enough in energy to show the peak of the $d\gamma$ band. At room temperature, photoconductivity shows a single absorption band having a maximum at 3.0 ev, probably the $d\epsilon$ band, and a broad shoulder at higher energy which may be the beginning of the $d\gamma$ band. The width of the main absorption band seems to be a few tenths of an

electron volt, which is very reasonable for a 3*d* band. At 103°K, this band gives an indication of splitting; this is not surprising, since the cation in the rutile structure is not at the center of a regular octahedron of anions.

4.2 *TiO* (*Configuration* d^2)

Besides TiO_2, the only oxide for which there is fairly clear evidence of a 3*d* band is TiO. This oxide behaves like a metal, indicating the existence of a partially filled 3*d* band. According to Pearson,[32] room-temperature conductivity is 3500 $ohm^{-1}cm^{-1}$ and increases slowly with decreasing temperature. Conductivity also decreases in a ratio of 7:12 when the oxygen content is increased from $TiO_{0.7}$ to $TiO_{1.2}$. This is to be expected if the effect of changing the stoichiometry is to produce an equal change in the number of 3*d* electrons in the 3*d* band. If all the 3*d* electrons, 6×10^{22} for stoichiometric TiO, are assumed to be involved in conduction, the electron mobility can be calculated to be $\mu = \sigma/qn = 3500/(1.6 \times 10^{-19} \times 6 \times 10^{22}) = 0.36$ cm^2/volt-sec at room temperature. This is comparable with the mobility in TiO_2 and suggests conduction in a 3*d* band in this case also.

4.3 *Ti_2O_3* (*Configuration* d^1) *and* *V_2O_3* (*Configuration* d^2)

Since these oxides contain, respectively, one and two 3*d* electrons per cation, metallic conduction is expected if a 3*d* band exists in them, just as in the case of TiO. Conductivity data for these oxides are shown in Figs. 11 and 12. The outstanding fact about these data is the large discontinuity in conductivity at T_N for a number of samples. (The lack of a discontinuity in some cases will be discussed later.) No other oxides have shown such behavior, and it is this behavior which suggests an energy band scheme that explains fairly well the information available for these oxides. To begin with, one expects the 3*d* band to be split by the crystal field into the $d\gamma$ and $d\epsilon$ sub-bands. It is proposed, further, that the $d\epsilon$ band may be split by the magnetic exchange interaction into a lower filled band and an upper empty band. Thus, in a pure stoichiometric sample at temperatures below T_N, the Fermi level would be midway between the occupied $d\epsilon$ band and the empty $d\epsilon$ band. When the temperature of the sample is raised through T_N, the bands would collapse into a single partially filled band and cause metallic conduction. Sample A of V_2O_3 behaves in this way. If it is assumed that carrier mobility does not change very much on going through T_N, and that the conductivity change is due only to the change in carrier concentration resulting from the collapsing of $d\epsilon$ bands, the amount of discontinuity

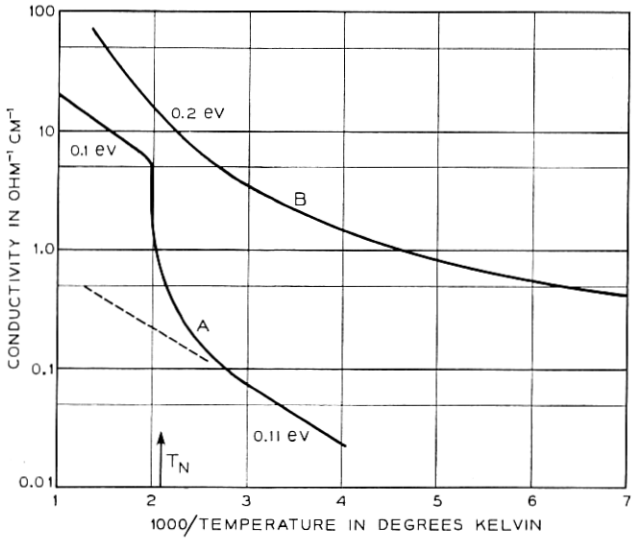

Fig. 11 — Conductivity of Ti_2O_3 through the Néel temperature. (Sample A, Foëx and Loriens, Ref. 45; sample B, Pearson, Ref. 32.)

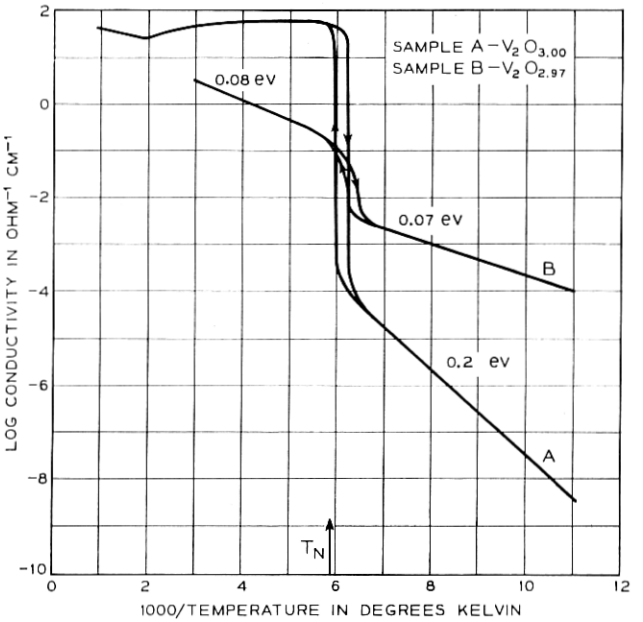

Fig. 12 — Conductivity of V_2O_3 through the Néel temperature. (After Foëx, Ref. 46.)

to be expected in the conductivity of a pure stoichiometric sample can be estimated. This will be simply a factor of exp (E_F/kT_N), where E_F is taken to be the slope of the conductivity curve below T_N. For V_2O_3 sample A, this factor is exp $(0.2/8.63 \times 10^{-5} \times 170) = 8 \times 10^5$, which is very close to the measured discontinuity. For Ti_2O_3 sample A, the factor is exp $(0.11/8.63 \times 10^{-5} \times 470) = 15$, again very close to the observed discontinuity, although this sample does not show metallic conduction above T_N. A remarkable point about these two cases is that the Fermi energy is changed at the discontinuity by an amount considerably greater than the exchange energy kT_N.

If a sample departs from stoichiometry several effects can be imagined which would work to obscure the discontinuity: the odd, or missing, cations in the lattice will tend to decouple the spin system; they may break up the periodicity of the lattice and disrupt the 3d band; they will alter the conductivity by acting as donors or acceptors. Samples A and B of Ti_2O_3 and V_2O_3 sample B probably show these effects in varying degrees. With the band disrupted, transport probably occurs as in oxides such as NiO, and metallic conduction does not appear above T_N. The presence of donors or acceptors increases the conductivity below T_N and minimizes the effect of the magnetic transition on the conductivity.

An estimate of electron mobility for V_2O_3 sample A above T_N gives $\mu = \sigma/qn = 60/(8 \times 10^{22} \times 1.6 \times 10^{-19}) = 5 \times 10^{-3}$ cm²/volt-sec. Thus, mobility in a single crystal may be of the order of 10^{-2}cm²/volt-sec, which is more than an order of magnitude less than in TiO_2 so that the 3d band in V_2O_3 is probably not much greater than kT in width at temperatures above T_N.

It seems reasonable to conclude from the considerations and results of this and the previous section that a 3d band exists in the oxides of scandium, titanium and vanadium, which probably goes to essentially zero width in chromium oxide. A schematic of this idea is shown in Fig. 13.

V. RELATIVE ENERGIES OF THE 4s, 3d AND 2p LEVELS

We saw in the last section that, of the 3d oxides, probably only those of Sc, Ti and V are like ordinary semiconductors in that their charge carriers are in energy bands. When we come to Cr_2O_3 and the remaining 3d oxides we find an entirely new situation. The 2p and 4s bands are quite comparable to the bands in ZnO, for example, and can be represented on the usual one-electron energy diagram. However, the energy of conduction electrons and holes in the localized 3d levels must be

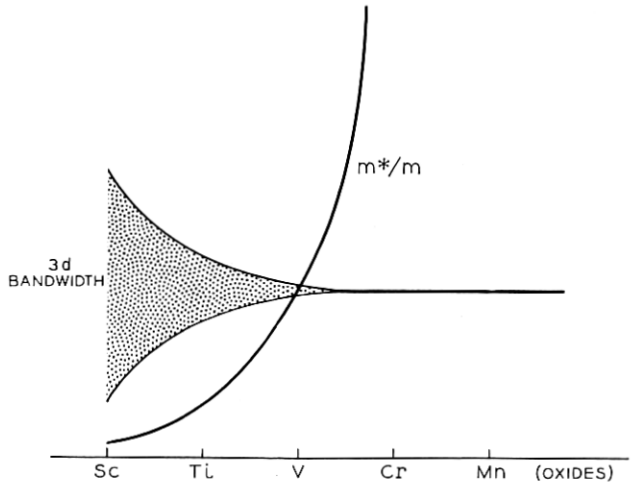

Fig. 13 — Schematic showing how 3*d* bandwidth goes to zero and effective mass, m^*/m, of charge carriers increases as 3*d* wave functions contract with increasing atomic number.

represented in a different way, since they are in excited states of the cation.

It is possible to find, in a very approximate way, the relative energies of the unbroadened 4*s*, 3*d* and 2*p* levels in an oxide by using data from the Born cycle, and spectroscopic data for the free ions and neglecting lattice polarization about an electron or hole. In Fig. 14, NiO is taken as an example to show how this is done.

Charge carriers are produced by the following reactions, in which the electronic states represented are separated by large distances in the crystal:

$$O^{--}(2p^6) + Ni^{++}(3d^8) \rightarrow O^{-}(2p^5) + Ni^{+}(3d^9), \tag{4}$$

$$Ni^{++}(3d^8) + Ni^{++}(3d^8) \rightarrow Ni^{+++}(3d^7) + Ni^{+}(3d^9), \tag{5}$$

$$NI^{++}(3d^8) \rightarrow Ni^{++}3d^7 4s \rightarrow Ni^{+++}(3d^7) + 4s \text{ electron}, \tag{6}$$

$$V\text{-}Ni^{+++}(3d^7) + Ni^{++}(3d^8) \rightarrow V\text{-}Ni^{++}(3d^8) + Ni^{+++}(3d^7), \tag{7}$$

$$Li^{+}Ni^{+++}(3d^7) + Ni^{++}(3d^8) \rightarrow Li^{+}Ni^{++}(3d^8) + Ni^{+++}(3d^7). \tag{8}$$

These reactions represent: (4) the formation of a hole in the 2*p* band and an electron in the 3*d* levels; (5) the formation of an electron-hole pair in the 3*d* levels; (6) the excitation of an electron to the 4*s* band and formation of a hole in the 3*d* levels; (7) the trapping of an electron at a lattice vacancy acceptor with the formation of a hole in the 3*d*

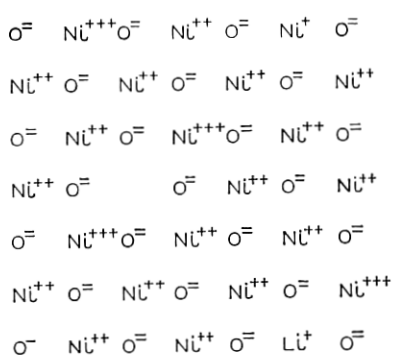

Fig. 14 — Lattice of NiO with Ni^{+++} acceptors near a cation vacancy and a substituted Li^+, Ni^+ electron and Ni^{+++} hole, and a O^- hole in the $2p$ band.

levels; and (8) the trapping of an electron at a Li^+ acceptor site with the formation of a hole in the $3d$ levels. Consider first the energy necessary to remove an electron from O^{--} and place it on a distant Ni^{++} in the lattice, as shown by reaction (4). The total electron affinity of an oxygen atom (O going to O^{--}), determined by the Born cycle, is repulsive and equals -7.5 ev.[33] The affinity of O for the first electron is $+2.2$ ev;[34] hence the negative affinity for both electrons is due to the affinity for the second electron ($O^- \rightarrow O^{--}$), which therefore amounts to -9.7 ev. This energy is plotted in Fig. 15 relative to the $2p^5$ level plus a free electron on the left of the energy diagram. The ionization potential of $Ni^+(3d^9)$ and the other spectroscopic data come from Ref. 28. This ionization potential is 18.2 ev, and it is plotted relative to the $3d^8$ level in the diagram. (These energies are plotted with reversed signs, since in the process being investigated an electron is to be taken from O^{--} and placed on the Ni^{++}, and this is the reverse of the process for which the energies are quoted.) When the ions are brought together to form the lattice, the potential at the position of a positive ion due to all the other ions in the lattice is negative, and that at the position of the negative ion it is positive. As a result, the O^{--} level is depressed and the Ni^{++} level is raised (as shown in the diagram) by the amount of the Madelung potential[33] of NiO, which is 23.8 ev. Thus we find these levels moved to -14.1 ev ($2p^6$) and $+5.6$ ev ($3d^9$). The difference in energy of these two levels, 19.7 ev, is the energy of reaction (4), and it was arrived at by considering only free ion potentials, which are a measure of the energy necessary to remove an electron from a free ion out to infinity. In this process, the electron would experience the potential of the ion all the way to infinity. In the lattice, however, the process is carried out in a dielectric, so the energy required for the reaction is reduced by the di-

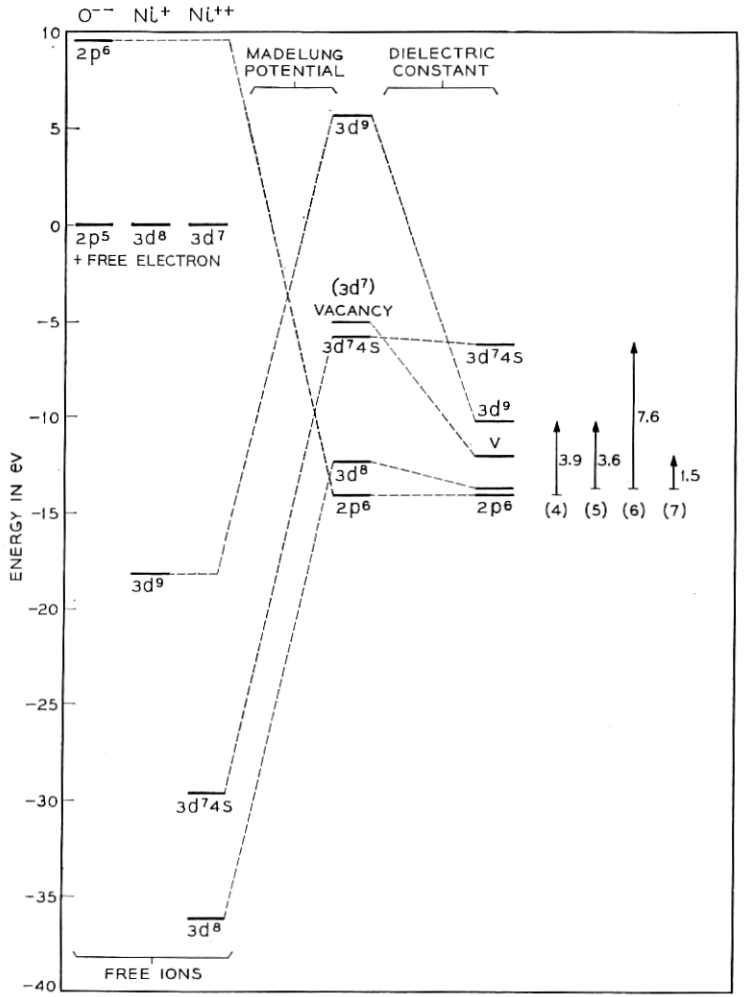

Fig. 15 — Energy level diagram calculated for NiO and showing the energy required for the reactions (4) through (7).

electric constant of NiO. Taking this constant to be about 5, the separation of the two levels is thus reduced to 19.7/5 = 3.9 ev, as shown on the diagram to the right in Fig. 15. This energy is probably reduced even further by broadening of the $2p$ levels into a $2p$ lattice band, so that the energy required to produce a free hole in the $2p$ band and an electron in the $3d$ levels is expected to be less than 3.9 ev, in NiO.

The next process of interest, given by reaction (5), is to take an electron

from a Ni^{++} and place it on another Ni^{++} far removed in the lattice. The $3d^8$ level is located at -36.2 ev, with respect to the $3d^7$ level in the left of the diagram. Adding to this the Madelung potential raises it to -12.4 ev. This lies 18.0 ev below the $3d^9$ level calculated in a similar manner in the preceding paragraph. In the lattice, therefore, the transition will require $18.0/5 = 3.6$ ev. Thus, on the right-hand side of the diagram the $3d^8$ level is plotted 3.6 ev below the $3d^9$ level which had been located in the first calculation.

Reaction (6) represents the transition of an electron from a Ni^{++} into the 4s band. The first step in calculating the energy required for this process is to take an electron from the ground state, $3d^8$, to the first excited 4s state, given by $3d^7 4s$. The location of this excited state with respect to the ground state is plotted to the left of the diagram, at -29.6 ev, and in the center, at -5.8 ev, by adding the Madelung potential, which places it 6.6 ev above the $3d^8$ level. Thus, it required 6.6 ev to produce this excited state of the cation, which is a bound hole-electron pair. The additional energy required to separate this pair (essentially to remove the electron from the field of the cation) is given approximately by $q^2/\epsilon a$, where ϵ is the dielectric constant and a is the distance between cations. This energy amounts to 1.0 ev, so that the energy required to free an electron from a cation and place it in a band of 4s states is 7.6 ev. This is plotted with respect to the $3d^8$ level at the right of the diagram. Due to broadening of the 4s levels into a band, the actual separation will be reduced to something less than 7.6 ev.

Consider now the process (7), in which excess oxygen in the NiO lattice introduces vacant Ni^{++} lattice sites, which act as acceptors and produce conduction holes in the 3d levels. The relative location in energy of such an acceptor level has been calculated by de Boer and Verwey,[7] although they neglected the effect of the dielectric constant of the solid. Their argument is as follows. Each vacant Ni^{++} site is surrounded by twelve Ni^{++} ions, and the situation to be considered is that in which two of these ions yield an electron each to form Ni^{+++} ions that compensate for the absence of the Ni^{++} ion. This is shown in Fig. 14. Each Ni^{+++} is surrounded by a normal lattice minus one Ni^{++} at a distance $a\sqrt{2}/2$, plus one positive charge (Ni^{+++}) assumed to be at $a\sqrt{2}$, the greatest separation from the first Ni^{+++}. Hence, the potential at one Ni^{+++} site amounts to the normal Madelung potential plus $2q^2/a\sqrt{2}/2 - q^2/a\sqrt{2} = 23.8 + 9.8 - 2.4 = 31.2$ ev. Thus, the level of this ion is raised 7.4 ev above that of the normal $3d^8$ ions, as shown in Fig. 15. Considering the dielectric constant, the energy required to transfer an electron from a distant Ni^{++} ion to a Ni^{+++} next to a vacancy will be

7.4/5 = 1.5 ev. This level is plotted to the right in Fig. 15 with respect to the $3d^8$ level. On this same basis, in reaction (8) a substitutional Li^+ will produce a Ni^{+++} acceptor level at 0.5 ev above the $3d^8$ level.

The calculated energies involving four of these reactions are shown by vertical arrows to the right of the diagram. They will be used in Sections VI and VII as guides in analyzing the data for NiO and Fe_2O_3. It will be seen in Section VI that these calculated energies are probably larger than the actual energies found in NiO by a factor of approximately two. Because of this, it is suggested that the dielectric constant of NiO is nearer to ten than to the value of five assumed in these calculations.

The Madelung potential is about the same for all the monoxides CuO through TiO. However, as we go from CuO to MnO, the second and third ionization potentials of the cation become progressively smaller. This raises the $3d$ levels in energy with respect to the $2p$ band. In MnO, for example, the $3d^3$ level is about 4.5 ev above the $2p$ band, as compared with a separation of 3.9 ev for the $3d^9$ level in NiO, (assuming a dielectric constant of five in both cases). Therefore, conduction by $2p$ holes may be less important in the oxides which are earlier in the series than is NiO.

Madelung constants are not available for the individual ions in the rhombohedral oxides where anions and cations do not occupy equivalent lattice sites. Therefore, the relative positions of the $3d$ levels and the $2p$ band in these oxides cannot be determined easily.

The location (as given in Ref. 22) of the $3d^n4s$ state with respect to the ground state in the free ion indicates that the $4s$ band becomes farther removed from the $3d$ levels as the charge on the cation is increased. Thus, the $4s$ band probably plays no role in conduction in any of the oxides having cations with a charge +2 or greater. The energy of the $3d-3d$ transition is given by the difference in ionization energy of the ground states, $3d^n$ and $3d^{n+1}$, divided by the dielectric constant of the oxide, as shown above for NiO. The only sesquioxide of interest here for which spectroscopic data are available is Cr_2O_3 (which is one that does not have a $3d$ band), for which the interval $3d^3 - 3d^4$ is 18.6 ev. This is about the same as $3d^8 - 3d^9$ in NiO.

The simple oxides, then, when pure and stoichiometric, can be expected to show conduction involving $3d$ holes and electrons and $2p$ holes, as a result of the processes shown in (4), (5) and (6). These are the processes corresponding to intrinsic conduction arising from excitation across the forbidden gap in the semiconductors discussed in earlier chapters. They will probably appear to be p-type, because conduction by high-mobility $2p$ holes will predominate over the conduction by low-mobility electrons in the $3d$ levels. On the other hand, when an oxide is impure or departs

from stoichiometry, as in (7) and (8), its type will depend, in addition to this intrinsic behavior, upon the particular valence state of the cation and upon the valence states available to the cation. It was shown above how excess oxygen or substitutional Li^+ in NiO introduced Ni^{+++} acceptor levels near to the $3d^8$ levels. In TiO_2, a departure from stoichiometry produces Ti^{+++} ions which are donors with respect to Ti^{++++} ions and introduce donor levels near to the 3d band. In general, when the cations are in their lowest valence state, a defect will be such as to cause the oxide to be p-type and, when the cations are in their highest valence state, a defect will be such as to cause the oxide to be n-type. Oxides such as Fe_2O_3, in which the cations are in an intermediate valence state, can be made to go either into n-type or p-type. However, at high temperatures even impure oxides will tend towards p-type, because of conduction by high mobility 2p holes. The energy levels discussed in Section III, of course, exist in addition to those shown in Fig. 15, but they are excited states which do not contribute to conduction.

VI. NICKEL OXIDE, NiO

Much more information is available for NiO than for the other cubic oxides, so it will be considered in detail. The structure of NiO has been described in Section II, and a possible electronic energy level scheme has

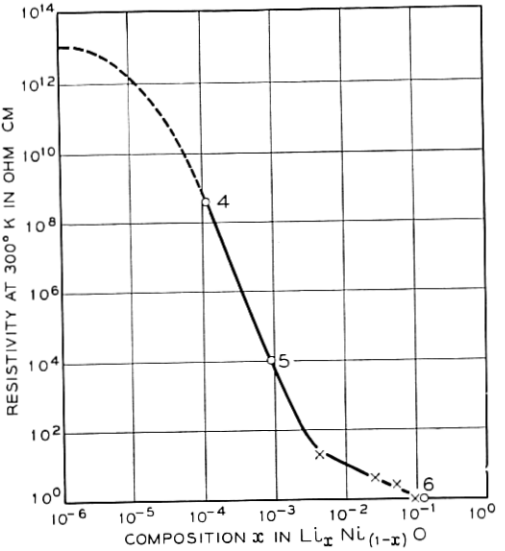

Fig. 16 — The resistivity of NiO as a function of Li content. (Sample o, Morin, Ref. 37; sample x, Verwey, Ref. 47.)

been discussed in Sections IV and V. Nickel oxide is a p-type semiconductor, apparently even when pure and stoichiometric, and no n-type form has been reported. Room-temperature resistivity for pure NiO is approximately 10^{13} ohm-cm. This can be lowered to about 1 ohm-cm by the addition of Li, as shown in Fig. 16.

The transport data available for NiO are from Wright and Andrews,[36] taken on oxidized pure Ni films, and Morin,[37] taken on sintered bars

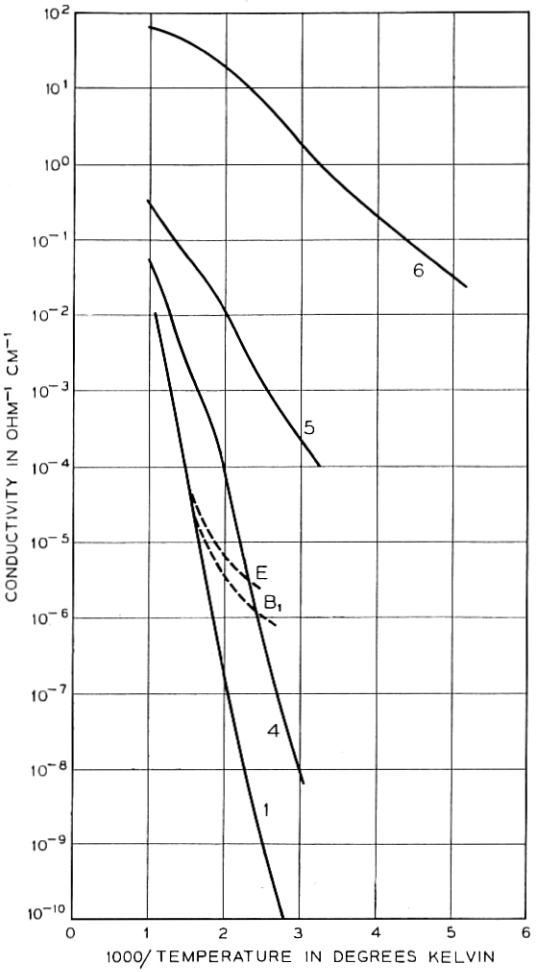

Fig. 17 — The conductivity of NiO (samples 1, B_1 and E) and of NiO containing Li (samples 4, 5 and 6; see Fig. 16). (Samples 1, 4, 5 and 6, Ref. 37; samples B_1 and E, Ref. 36.)

containing different amounts of Li and also presumed to vary in oxygen content. The data are shown in Figs. 17, 18 and 19. Samples 1 and B_1, judging from the method of preparation (see Refs. 36 and 37), their color (pale green) and their electrical behavior, are considered to be the purest and most nearly stoichiometric. Conductivity and thermoelectric effect of the other samples approaches that for these at high temperatures. This occurs in a way typical of semiconductors when impurity centers become completely ionized and intrinsic conduction predominates. In the intrinsic range, both Hall effect and thermoelectric effect remain *p*-type.

According to the calculations of Section V, the energy level diagram, Fig. 20 can be constructed. Three parallel conduction processes are expected for NiO, from reactions (4) and (5): σ_1, high-mobility $2p$ holes; σ_2, low-mobility $3d$ holes; and σ_3, low-mobility $3d$ electrons, so that total conductivity is given by

$$\sigma = \sigma_1 + \sigma_2 + \sigma_3 . \tag{9}$$

Carrier concentration will be given, choosing $E_1 = 0$ as the zero of energy,

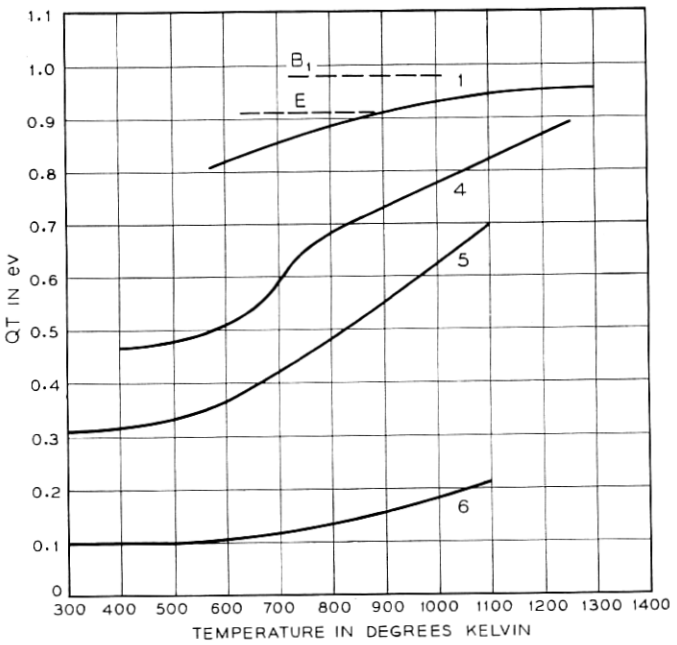

Fig. 18 — The Seebeck effect of NiO (samples 1, B_1, and E) and NiO containing Li (samples 4, 5 and 6; see Fig. 16). (Samples 1, 4, 5 and 6, Ref. 37; samples B_1 and E, Ref. 36.)

by

$$p_1 = 2\left(\frac{2\pi m^* kT}{h^2}\right)^{3/2} \exp(-E_F/kT), \tag{10}$$

$$p_2 = N \exp[-(E_F - E_2)/kT], \tag{11}$$

$$n_3 = N \exp[-(E_3 - E_F)/kT], \tag{12}$$

where N is the number of cations per cu cm. No Hall effect is expected from carriers p_2 and n_3 in localized $3d$ levels, and none has been observed. Under conditions of sufficiently high purity and stoichiometry, or at elevated temperature where an appreciable fraction of the current is carried by $2p$ holes, a Hall effect due to these holes is expected. Since such a Hall effect is due only to $2p$ holes, but the current is carried by three kinds of carriers, the Hall coefficient is given by

$$R_H = \frac{p_1 \mu_1^2}{(p_1 \mu_1 + p_2 \mu_2 + n_3 \mu_3)^2 q}. \tag{13}$$

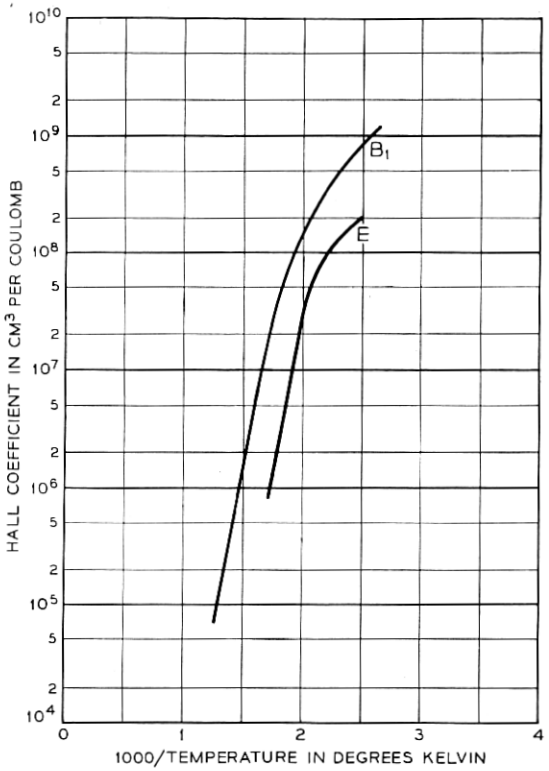

Fig. 19 — The Hall coefficient of NiO. (Samples B_1 and E, Ref. 36.)

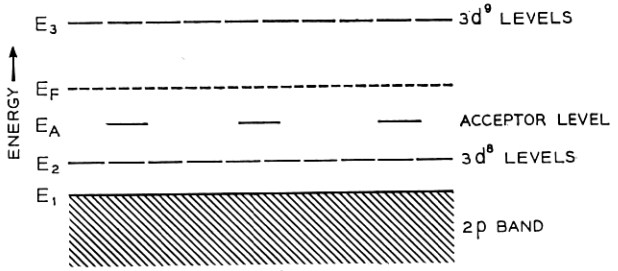

Fig. 20 — Energy level diagram proposed for NiO.

Because the 3*d* carriers give no Hall effect, their behavior has been studied using another tool, the Seebeck effect. In interpreting the Seebeck effect of the 3*d* oxides it is assumed that 3*d* carriers transport no kinetic energy, since they spend most of their time trapped on lattice sites. Therefore, there is no phonon drag effect associated with them, and their Seebeck effect is due only to their separation in energy from the Fermi level. For simplicity, it is assumed that there is no phonon drag effect associated with 2*p* holes. This assumption is probably a good one, since most of the data have been taken at elevated temperatures where this effect is at a minimum. The 2*p* holes are assumed to carry a kinetic energy of $2kT$. The over-all thermoelectric effect produced by three kinds of carriers is given by

$$QT\sigma = Q_1T\sigma_1 + Q_2T\sigma_2 - Q_3T\sigma_3 \tag{14}$$

or

$$QT\sigma = (E_F - E_1 + 2kT)\sigma_1 + (E_F - E_2)\sigma_2 - (E_3 - E_F)\sigma_3 . \tag{15}$$

The problem is to determine three carrier concentrations and three mobilities from only three independent experiments. This complicated calculation will not be attempted here. Rather, two extreme situations will now be assumed: (a) NiO doped with so much Li that only 3*d* holes contribute to conduction, and (b) NiO so pure that 2*p* holes predominate in conduction.

In Fig. 16 it is shown that the conductivity changes in direct proportion to the amount of Li added, for high concentrations of Li. One infers from this that each Li added contributes one hole to conduction and that nearly all the impurity centers are ionized. Thus, conduction is entirely extrinsic and due to 3*d* holes. Under these simplified conditions, (9) and (14) reduce to

$$\sigma = \sigma_2 \tag{16}$$

and

$$QT = (E_F - E_2). \tag{17}$$

Knowing now, from (17), the location of the Fermi level with respect to the $3d^8$ levels, the concentration, p_2, of $3d$ holes can be calculated from equation (11) if the density of states, N, available to the holes is known. This is assumed to be the number of cations per cu cm of crystal, which is 5.6×10^{22} in NiO, since we are dealing with holes localized on the cations rather than in an energy band.

Now, with the measured σ and the hole concentration calculated in this way from QT for sample 6, the mobility, μ_2, of the $3d^8$ holes has been calculated and is plotted in Fig. 21. Both in magnitude and in temperature dependence this result is in accord with the ideas concerning transport in highly localized $3d$ orbitals discussed in Sections I and VIII. Mobility at 300°K is 0.004 cm²/volt-sec and increases exponentially with temperature, with an activation energy of 0.10 ev. At low temperatures, QT (sample 6) is constant with temperature, at 0.10 ev. If the Fermi level lies halfway between the $3d^8$ levels and the acceptor states, this would indicate then that the [Li^+ Ni^{+++}] acceptor levels are 0.20 ev above the $3d^8$ levels in this sample, as compared with the value of 0.5 ev calculated in Section V and shown in Fig. 15. This suggests that a somewhat higher value should have been closen for the dielectric constant

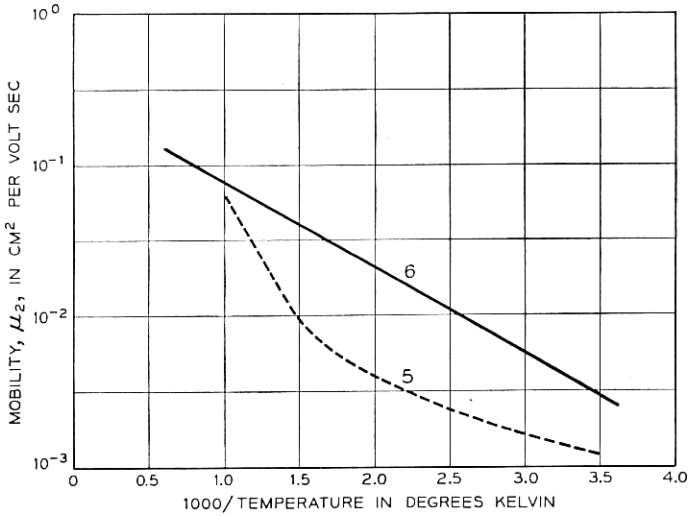

Fig. 21 — The mobility of holes in the $3d^8$ levels of NiO obtained from measurement of conductivity and Seebeck effect. (See Fig. 16 for composition of samples 5 and 6.)

in these calculations. On the other hand, at the high density of defects existing in sample 6, interaction among defects may occur, and this would reduce their ionization energy.

A calculation of p_2 and μ_2 has been made for sample 5, in which the [Li^+] is not in the range where σ_2 is directly proportional to [Li^+] (see Fig. 16). The mobility results are shown as a dashed line in Fig. 21. At temperatures for which $1/T$ is $>1.5 \times 10^{-3}$ they are parallel to, but much lower than, the results for sample 6; at higher temperatures they rise rapidly with temperature. It is assumed that transport of holes in the $3d^8$ levels consists of Ni^{++} states drifting by jumps from one cation to a neighbor cation under the influence of the applied electric field. Therefore, it seems likely that mobility for this type of transport will be independent of impurity concentrations. In fact, this is suggested in Fig. 16 by the direct proportionality between conductivity and Li concentration for high-Li concentration. Consequently, the results on sample 5 probably mean that conduction in the $2p$ band is appreciable in this sample and cannot be neglected in any sample containing less than a 3×10^{-3} atom fraction of Li (or approximately 2×10^{20} Li atoms/cm^3). This suggests, further, that the $2p$ band is not much farther below E_F than are the $3d^8$ levels, in accord with the energy level diagram in Fig. 15.

Now assume the second situation, pure NiO, with only $2p$ holes involved in conduction and $\mu_1 = R_H\sigma$. This result for sample E is shown in Fig. 22. Also, from this assumption (15) reduces to

$$QT = (E_F + 2kT). \tag{18}$$

From this, p_1 can be calculated from (10), assuming $m^*/m = 1$. Since $\sigma_1 = \sigma$, μ_1 can again be calculated. This has been done for samples 1 and B_1 and is also plotted in Fig. 22. There, the μ_1 results are compared with μ_L, a lattice-scattering mobility considered reasonable for carriers in the wide band of an oxide. The high values found for μ_1 support the idea that $2p$ holes are involved in the conduction. The temperature dependence that is found is quite far from a reasonable one, showing that the other conduction processes also play a role in these samples and cannot be neglected. These results, then, do not represent true $2p$ hole mobility. They do indicate, however, that the energy level scheme proposed for NiO is a reasonable one. With this model in mind, the QT results of Fig. 18 can be understood in a qualitative way. At low temperature, E_F is midway between E_2 and E_A, the acceptor levels, so that $\sigma = \sigma_1 + \sigma_2$. As the temperature is raised, E_F moves upward through E_A as acceptors become completely ionized, and QT increases accordingly.

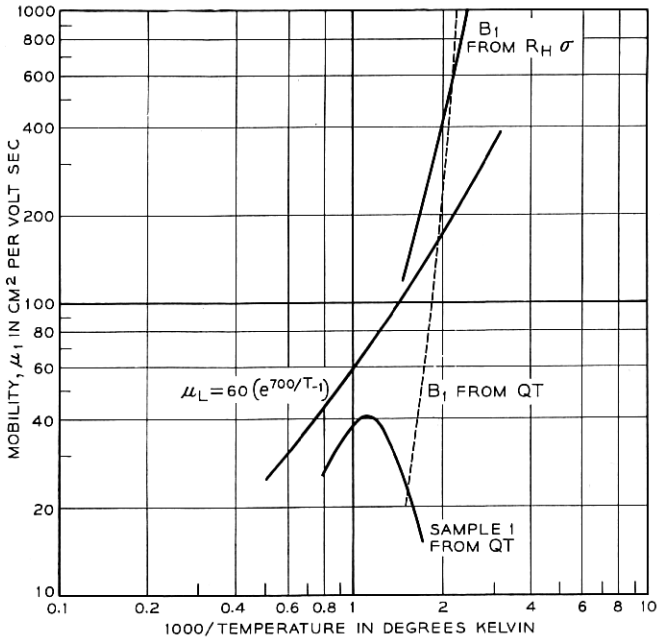

Fig. 22 — The mobility of holes in the $2p$ band of stoichiometric NiO obtained from measurement of conductivity Hall effect and Seebeck effect.

Finally, at high temperatures, all the acceptors become ionized in the purest samples, E_F lies nearly midway between E_2 and E_3, and QT becomes constant with temperature. Under these conditions, $Q_2T\sigma_2 - Q_3T\sigma_3$ approaches zero, and QT is p-type, due largely to $2p$ holes. At high temperature, measured QT for samples 1 and B_1 is about 1 ev. Furthermore, the slope of the conductivity and Hall coefficient plots for these two samples is also about 1.0 ev at high temperature. These results suggest that the $2p$ band is about 1.0 ev below the Fermi level in the intrinsic situation and, therefore, that the energy levels of Fig. 15 should be scaled down by a factor of one-half. This is also in fair agreement with the finding that the [Li^+ Ni^{+++}] acceptor level lies 0.2 ev above the $3d^8$ level rather than 0.5 ev above, as was calculated. Evidently the value of ten would have been a better assumption for the dielectric constant of NiO.

VII. IRON OXIDE, Fe_2O_3

Magnetic and structural properties of the rhombohedral sesquioxide of iron have been described in Section II. Its semiconductor behavior is very similar to that of NiO, except that Fe_2O_3 can exist as either n- or

p-type because the cation can take on a lower as well as a higher valence state. Oxidation causes pure Fe_2O_3 to become *p*-type, probably due to the production of Fe^{++++} ions in the vicinity of cation vacancies. Reduction causes pure Fe_2O_3 to become *n*-type, probably due to the production of excess cations in the form of Fe^{++} ions. With respect to the normal lattice of Fe^{+++} ions, Fe^{++++} is a hole and Fe^{++} an electron. The room-temperature resistivity of Fe_2O_3 is approximately 10^{13} ohm-cm. This can be lowered to about 4 ohm-cm by the addition of Ti. It is known from an X-ray study[38] that, in the isomorphous compound $FeTiO_3$, the cations are Fe^{++} and Ti^{++++} at room temperature. Presumably then, Ti^{+++} in Fe_2O_3 also ionizes, to give a 3*d* electron (Fe^{++}) and a Ti^{++++} ion. The change in resistivity with added Ti is shown in Fig. 23. At high Ti concentrations the resistivity does not decrease with added Ti. This may be due to a shifting oxygen equilibrium with Ti content, which introduces acceptors that compensate for some of the donors.

Transport data[18, 39] available for Fe_2O_3 have been obtained on sintered bars, and consist of conductivity, Fig. 24, and thermoelectric effect, Fig. 25. Samples 1 and A are identical in conductivity, but the thermoelectric effect shows that, due to the different conditions of sintering, sample 1 is *p*-type and sample A is *n*-type. The *QT* data also show that both of these samples tend to be *p*-type at high temperatures, which is in accord with (14) and the idea that the general energy level scheme which was developed in Section V for NiO is probably applicable to most of the simple oxides. However, in Fe_2O_3, *QT* is smaller in the intrinsic range than it is in NiO. This suggests that the 3*d* levels in Fe_2O_3 are higher above the 2*p* band than they are in NiO.

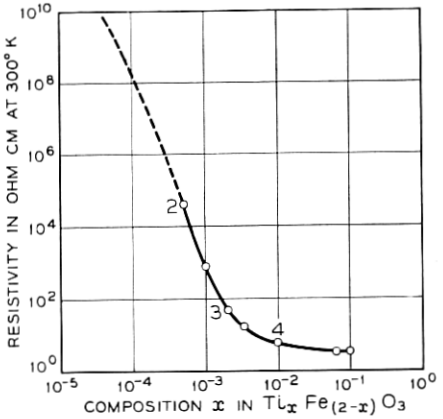

Fig. 23 — The resistivity of Fe_2O_3 as a function of Ti content. (Ref. 18).

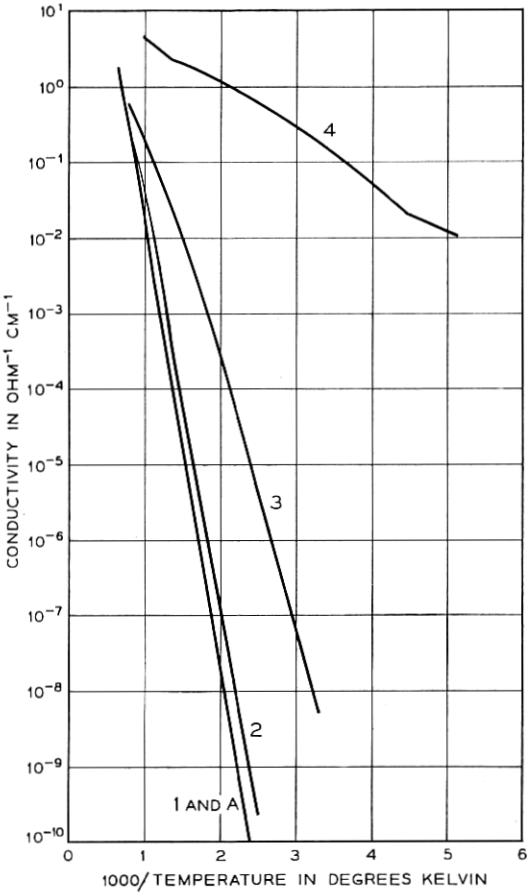

Fig. 24 — The conductivity of Fe_2O_3 (samples 1, A and 2) and Fe_2O_3 containing Ti (samples 3 and 4; see Fig. 23 for composition).

The situation in Fe_2O_3, where both donors and acceptors are present, is somewhat more complicated than in NiO. However, the simple case in which Fe_2O_3 is so heavily doped with Ti that conduction is only by $3d$ electrons can be dealt with. Such a situation is probably represented by sample 4, in which

$$\sigma = \sigma_3 , \tag{19}$$

$$QT = (E_3 - E_F), \tag{20}$$

and n_3 is given by (12), where $N = 4.0 \times 10^{22}$ cm^{-3}. From these equations and the data for sample 4, μ_3 has been determined. It is found to

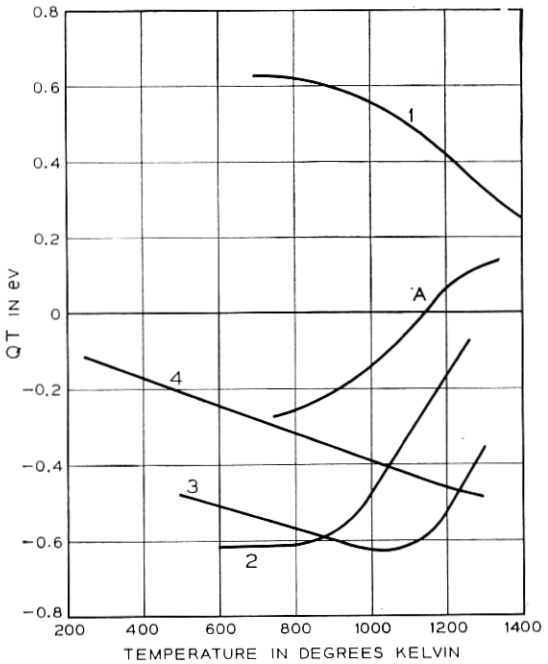

Fig. 25 — The Seebeck effect of Fe_2O_3 (samples 1, A and 2) and Fe_2O_3 containing Ti (samples 3 and 4; see Fig. 23 for composition).

be identical with the hole mobility for NiO sample 6, shown in Fig. 21. Thus the mobility of 3*d* electrons in Fe_2O_3 is in accord, both in magnitude and temperature dependence, with the idea of transport in localized 3*d* levels. At $T = 300°K$, $\mu_3 = 0.004$ cm²/volt-sec and increases exponentially with temperature with an activation energy of 0.1 ev.

VIII. TRANSPORT IN THE 3*d* LEVELS

In Section V the processes were described by which conduction electrons or holes are created in the 3*d* levels. In NiO, for example, a 3*d* hole freed from a cation defect is presumed to consist of a Ni^{+++} with the cation neighbors for some distance around it normal Ni^{++} ions. The hole can diffuse about the cation lattice by exchanging an electron with a Ni^{++} neighbor until it moves next to an ionized defect site, receives an electron and becomes trapped, or until it becomes annihilated by recombination with a free electron. A net drift of such holes occurs when an external electric field is applied to the crystal, and thus an electric current is obtained.

In Sections VI and VII the mobility of 3*d* charge carriers was shown

to be very low and to increase exponentially with temperature. These results are consistent with a suggestion made 20 years ago by de Boer and Verwey[7] that conduction in NiO and Fe_2O_3 occurs as outlined above and that a potential barrier exists which must be overcome for a charge carrier to jump from one cation to another. The potential barrier is assumed to arise because the charge carrier spends a time on a particular cation which is long compared to the vibrational frequency of the lattice, and this allows the ions surrounding a charge carrier to become displaced by its electric field. Evidence that this occurs in Fe_2O_3 containing Ti was given in Section III. This displacement creates a field which tends to prevent the charge carrier from leaving its lattice site, and so the charge carrier has trapped itself.[40, 41] These ideas can be represented by two energy levels, one for a hole, the other for a normal cation neighbor, being moved up and down in energy by phonons. Whenever the two levels become the same, charge transfer can occur; thus, an exponential temperature dependence would be found for transport.

One might expect this charge transfer to depend upon the electron configuration of the cation. Using the diagram in Fig. 6 one can see that, if Hund's rule* is followed, a hole in MnO and CuO will be in the $d\gamma$ levels but a hole in FeO, CoO and NiO will be in the $d\epsilon$ levels. Now, since the $d\epsilon$ orbitals are directed between anions and towards neighboring cations while $d\gamma$ orbitals are directed at anions, transport in the two levels may be quite different. For example, transport in the $d\gamma$ levels, through an anion as in superexchange, will involve spin reversal below T_N regardless of crystal orientation. Transport in the $d\epsilon$ levels will not involve spin reversal if it is in the (111) planes of parallel spins but will require spin reversal if it is perpendicular in the planes of parallel spin, and it so may produce an anisotropy in conductivity, at least within a magnetic domain.

If spin reversal is involved in transport, one might expect the activation energy for transport below T_N to be the sum of the polarization energy plus the exchange energy, and to be only the polarization energy above T_N. This would introduce an abrupt change in the temperature dependence of conductivity at T_N. Heikes and Johnston[42] believe that they have seen this effect in sintered samples of the oxides MnO, CoO, NiO and CuO which contained a large concentration of Li. However, the results described in Section VI for NiO containing Li (sample 6) show no change in the slope of mobility (Fig. 20) at T_N, but do show

* That the d levels are filled with electrons in such a way as always to maintain a maximum spin multiplicity.

that the slope of conductivity is changing in this temperature region, because the Fermi level (Fig. 18) is beginning to move upward. It is evident that these questions can be answered only by transport studies on single crystals.

ACKNOWLEDGMENTS

The author wishes to thank P. W. Anderson, C. J. Ballhausere, A. D. Liehr and G. H. Wannier for many helpful discussions and N. B. Hannay for editing the manuscript.

REFERENCES

1. Becker, J. A., Pearson, G. L. and Green, C. B., Trans. A.I.E.E., **65,** 1946, p. 711.
2. Gorter, E. W., Proc. I.R.E., **43,** 1955, p. 1945.
3. Emmett, P. H., *Catalysis*, Vol. 2, Reinhold Publ. Co., New York, 1955.
4. Evans, U. R., *Metallic Corrosion, Passivity and Protection*, Edward Arnold & Co., London, 1937.
5. Slater, J. C., *Handbuch der Physik*, Vol. 19, J. Springer, Berlin, 1956.
6. Coster, D. and Kiestra, S., Physica, **14,** 1948, p. 175.
7. de Boer, J. H. and Verwey, E. J. W., Proc. Phys. Soc. (London), **49,** 1937, p. 66
8. Mott, N. F., Proc. Phys. Soc (London), **62A,** 1949, p. 416.
9. Nagamiya, T., Yosida, K. and Kubo, R., Phil. Mag. Suppl. **4,** 1955, p. 1.
10. Anderson, P. W., Phys. Rev., **79,** 1950, p. 350.
11. Yamashita, J. and Kondo, J., Phys. Rev. **109,** 1958, p. 730.
12. Shull, C. G., Stauser, W. A. and Wollan, E. O., Phys. Rev., **83,** 1951, p. 333; Brockhouse, B. N., J. Chem. Phys. **21,** 1953, p. 961.
13. McGuire, T. R., Scott, E. J. and Grannis, F. H., Phys. Rev. **102,** 1956, p. 1000.
14. Néel, L. and Pauthonet, R., Comptes Rendus, **234,** 1952, p. 2172.
15. Anderson, P. W., Merritt, F. R., Remeika, J. P. and Yager, W. A., Phys. Rev. **93,** 1954, p. 717.
16. Néel, L., Ann. de Phys. **4,** 1949, p. 249.
17. Dzyaloshinski, J. B., J.E.T.P. (USSR), 1957, p. 1547; and J. Phys. Chem. Solids, **4,** 1958, p. 241.
18. Morin, F. J., Phys. Rev., **83,** 1951, p. 1005.
19. Karplus, R. and Luttinger, J. M., Phys. Rev., **95,** 1954, p. 1154.
20. Smart, J. S. and Greenwald, S., Phys. Rev. **82,** 1951, p. 113; Kanamori, J., Prog. Theo. Phys., **17,** 1957, pp. 177 and 197.
21. Greenwald, S., Nature, **168,** 1951, p. 379.
22. Moffitt, W. and Ballhausen, C. J., Ann. Rev. Phys. Chem., **1,** 1956, p. 197.
23. Van Vleck, J. H., J. Chem. Phys., **3,** 1935, p. 807.
24. Pauling, L., *The Nature of the Chemical Bond*, Cornell Univ. Press, Ithaca, N. Y., 1948.
25. Orgel, L. E., J. Chem. Phys., **23,** 1955, p. 1004.
26. Van Vleck, J. H., J. Phys. Chem., **41,** 1941, p. 67.
27. Ilse, F. E. and Hartmann, H., Z. für Physik. Chem., **197,** 1951, p. 239.
28. *Atomic Energy Levels*, N. B. S. Circular 467, Vols. 1949 and 1952.
29. Van Santen, J. H. and Van Wieringen, J. S., Rec. Trav. Chem, **71,** 1952, p. 420; Hush, N. S. and Price, M. H. L., J. Chem. Phys., **28,** 1958, p. 244.
30. Breckenridge, R. G. and Hosler, W. R., Phys. Rev., **91,** 1953, p. 793.
31. Cronemeyer, D. C., Phys. Rev., **87,** 1952, p. 376.
32. Pearson, A. D., M. I. T. Lab for Insul. Res. Tech. Report 120, 1957.
33. Sherman, J. J., Chem. Revs. **11,** 1932, p. 93.
34. Lozier, W. W., Phys. Rev., **46,** 1934, p. 268.
35. Gilleo, M. A., Phys. Rev. **109,** 1958, p. 777.

36. Wright, R. W. and Andrews, J. P., Proc. Phys. Soc. (London), **62A,** 1949, p. 446.
37. Morin, F. J., Phys. Rev., **93,** 1954, p. 1199.
38. Barth, T. F. W. and Posnjak, E., Z. Krist. **88,** 1934, p. 265.
39. Morin, F. J., Phys. Rev., **93,** 1954, p. 1195.
40. Mott, N. F. and Gurney, R. W., *Electronic Processes in Ionic Crystals*, Clarendon Press, Oxford, England, 1950.
41. Yamashita, J. and Kunosawa, T., J. Chem. Phys. Solids, **5,** 1958, p. 34.
42. Heikes, R. R. and Johnston, W. D., J. Chem. Phys., **26,** 1957, p. 582.
43. Holmes, O. G. and McClure, D. S., J. Chem. Phys., **26,** 1957, p. 1686.
44. Goldschmidt, V. M., *Internationale Tabellenzur Bestimmung von Kristallstrukturen*, Vol. 2, Berlin, 1935.
45. Foëx, M. and Loriens, J., Comptes Rendus, **226,** 1948, p. 901.
46. Foëx, M., J. des Rech. du C.N.R.S., **21,** 1952, p. 237.
47. Verwey, E. J. W., Chem. Weekblad, **44,** 1948, p. 705.